Advances in Computational Mathematics 2(1994)23–40

Elastic curves on the sphere

Guido Brunnett
FB Informatik, Universität Kaiserslautern, Postfach 3049, 6750 Kaiserslautern, Germany

and

Peter E. Crouch
Center for Systems Science and Engineering, Arizona State University, Tempe, AZ 85287, USA

This paper deals with the derivation of equations suitable for the computation of elastic curves on the sphere. To this end, equations for the main invariants of spherical elastic curves are given. A new method for solving geometrically constraint differential equations is used to compute the curves for given initial values. A classification of the fundamental forms of the curves is presented.

1. Introduction

In Euclidean space, an *elastic curve* can be viewed as an arc length parametrized "cubic" spline in tension, i.e. an elastic curve is a critical point of the functional

$$\Phi(y) = \int_0^l \langle y'', y'' \rangle + \sigma \langle y', y' \rangle \, ds \tag{1}$$

in the space F of smooth maps

$$y : [0, l] \to \mathbb{R}^n, \quad |y'| = 1,$$
$$y(0) = P_0, y(l) = P_1, y'(0) = V_0, y'(l) = V_1,$$

where $P_0, P_1 \in \mathbb{R}^n$, $V_0 \in T_{P_0}\mathbb{R}^n$, $V_1 \in T_{P_1}\mathbb{R}^n$, $\sigma \in \mathbb{R}$ are fixed and l is variable. Expressing y'' in the Frenet frame yields the functional Φ in the form

$$\Phi(y) = \int_0^l (\kappa(s))^2 + \sigma \, ds, \tag{2}$$

where κ denotes the curvature of y.

According to Bernoulli, the strain energy of an idealized one-dimensional elastic material is proportional to (2), which explains the interest in elastic curves as those curves that minimize bending (see [14]). In geometric modeling, the need for interpolants of high technical smoothness has revived the interest in elastic curves. To model smooth shapes, Minimal Energy Splines (MES), i.e. curvature continuous segmented curves with elastic curves as segments, have been proposed and successfully implemented (see [2,3,5,13,15]).

Spline techniques on the sphere have been developed to solve spherical interpolation problems, e.g. in the context of computer animation (see [18,16,11]). Open problems with spherical splines include the construction of splines of continuity higher than C^1, of proper parametrization, and of technical smoothness. The Euclidean MES possesses all three of these properties, which is a consequence of the variational principle involved. This suggests to consider spherical curves defined as solutions of the analogous variational problem for curves on the sphere.

Another application and motivation for this work comes from the field of control theory. Two important problems arise. In optimal control one wishes to choose an optimal trajectory for a control system by suitable choice of the control function, to minimize (maximize) an integral cost function along trajectories of the system. In the problem of path planning one wishes to simply choose one curve that joins two points in phase space. It is often desirable to accomplish both objectives simultaneously, but this is usually difficult in practice. A conceptually simpler procedure, which is now achieving some attention, is to generate curves by piecing together optimal trajectories, relative to a cost functional, just as in the classical interpolation setting of geometric modeling. However, in this case the curves are comprised of pieces of trajectories generated by a control system, not the usual cubic splines. This procedure has been named "dynamic interpolation" (see [12]).

In many applications, such as occurs in robotics and aerospace, the dynamics is constrained to a geometric object, such as a Lie group, e.g. multiple copies of the Euclidean group, or a homogeneous space, e.g. a sphere. Thus, one poses the problem of dynamic interpolation on such spaces. The simplest dynamic interpolation problem that one can pose on the sphere results in the variational problem addressed here. The aim of the interpolation problem would then be to join arbitrary pairs of points on the sphere by pieces of the trajectories derived in this work, but this is another unsolved problem.

In this paper, we derive the equations of spherical elastica and establish methods for the efficient computation of these curves. The presented material is divided into four sections.

Section 2 gives a brief review of geometric preliminaries.

In section 3, a set of differential equations for elastic curves on the sphere is derived. This set includes a differential equation for the geodesic curvature of spherical elastica. Since the normal curvature of a spherical curve is constant, the differential equation for the geodesic curvature suffices to compute the ordinary

curvature of a spherical elastica. Furthermore, a formula is given that expresses the squared torsion of a spherical elastica as a rational function of its curvature.

In section 4, we describe the numerical algorithm used to integrate the set of differential equations derived in section 3. The equations have a very particular structure defined by a number of constants of motion, and in particular they constrain the elastic curves to lie on the sphere. We employ an algorithm introduced by Crouch and Grossman [9] which preserves the constraints exactly.

Since Euler's fundamental work on plane elastic curves, it has been known that these curves can be classified according to their shape. The tools developed in this paper enable us to present the fundamental forms of spherical elastica in the last section.

2. Geometric preliminaries

Let $S : U \subset \mathbb{R}^2 \to \mathbb{R}^3$ denote a regular parametric surface and N the unit normal vector field of S. A curve $x : I \subset \mathbb{R} \to \mathbb{R}^3$ is a curve on the surface S if and only if $x = S \circ c$, where $c : I \to U$ is a plane curve in U. The unit normal of S along a surface curve x will be denoted by $n := N \circ c$.

The *Darboux frame* b_1, b_2, b_3 along x is the orthogonal frame defined by

$$b_1(t) = \frac{x'(t)}{|x'(t)|}, \quad b_2(t) = n(t) \times b_1(t), \quad b_3(t) = n(t).$$

The equations that express the derivatives b_1', b_2', b_3' in the Darboux basis b_1, b_2, b_3 are given by

$$b_1' = \omega\kappa_g b_2 + \omega\kappa_n b_3, \tag{3}$$

$$b_2' = -\omega\kappa_g b_1 + \omega\tau_g b_3, \tag{4}$$

$$b_3' = -\omega\kappa_n b_1 - \omega\tau_g b_2, \tag{5}$$

with $\omega(t) = |x'(t)|$.

The functions κ_g, κ_n and τ_g are called geodesic curvature, normal curvature and geodesic torsion. The geodesic torsion and the absolute value of geodesic and normal curvature are invariant under reparametrization of the surface.

The geodesic curvature of a surface curve x at a point $x(t)$ is the ordinary curvature of the plane curve generated by orthogonal projection of x onto the tangent plane of S at $x(t)$. It can be computed using the formula

$$\kappa_g = \frac{[x', x'', n]}{|x'|^3}. \tag{6}$$

A surface curve with identically vanishing geodesic curvature is called a *geodesic* of the surface.

The absolute value of the normal curvature of x at a point $x(t)$ is the curvature of the intersection of S with the plane through $x(t)$ spanned by the vectors $x'(t)$ and $n(t)$. While the geodesic curvature is the curvature of a surface curve from a viewpoint in the surface, normal curvature measures the curvature of the curve that is due to the curvature of the underlying surface. If κ denotes the ordinary curvature of the space curve s, the identity

$$\kappa^2 = \kappa_n^2 + \kappa_g^2 \tag{7}$$

holds.

The geodesic torsion of a surface curve x at a point $x(t)$ is the torsion of the geodesic that meets x at $x(t)$ with common tangent direction. A *curvature line* of x, i.e. a curve with a tangent vector that points into one of the principal directions of the surface, is characterized by vanishing geodesic torsion.

3. The differential equations of elastic curves on the sphere

The notion of cubic splines can be generalized to curves on a Riemannian manifold M by replacing the usual derivative of the tangent vector field y' by the covariant derivative compatible with the metric of M (see [17]). Generalizing the functional (1) in this way, one obtains the concept of elastic curves on arbitrary manifolds. In the case of surfaces embedded in $\mathbb{R}^3$, the algebraic value of the covariant derivative of the tangent vector field y' of a surface curve y is the geodesic curvature κ_g of y (see [6]). Therefore, we may define an elastic curve on a surface $S : A \subset \mathbb{R}^2 \to \mathrm{S} \subset \mathbb{R}^3$ as an extremal point of the functional

$$\Phi(y) = \int_0^l (\kappa_g(s))^2 + \sigma \, ds, \tag{8}$$

in the space $\overline{F}$ of C^∞ smooth maps

$$y : [0, l] \to \mathrm{S}, \quad |y'| = 1,$$

$$y(0) = P_0, y(l) = P_1, y'(0) = V_0, y'(l) = V_1,$$

where $P_0, P_1 \in \mathrm{S}$, $V_0 \in T_{P_0}\mathrm{S}$, $V_1 \in T_{P_1}\mathrm{S}$, $\sigma \in \mathbb{R}$ are fixed and l is variable.

Let S be a parametrization of a patch on the sphere $\mathrm{S}_2 \subset \mathbb{R}^3$ of radius r and center 0 such that

$$S = rN$$

and x be an arc length parametrized (i.e. $|x'| = 1$) curve on S. Then

$$x' = rn' = rb_3'.$$

In this situation, (5) implies that

$$\kappa_n = -\frac{1}{r}, \quad \tau_g = 0. \tag{9}$$

Since the absolute values of κ_n and τ_g are invariant under reparametrization, these equations imply that any spherical curve is a curvature line with constant normal curvature.

From (3), one obtains the relation

$$|b_1'|^2 = \kappa_g^2 + \frac{1}{r^2},$$

so that we wish to minimize the functional

$$\int_0^l |b_1'(s)|^2 + \delta \, ds,$$

where

$$\delta = \sigma - \frac{1}{r^2}$$

under the constraints

$$|b_1|^2 = 1, \quad b_1 = x', \quad |x|^2 = r^2.$$

Hence, we can apply the Euler–Lagrange equations to the functional

$$F = |b_1'|^2 + \delta + \lambda(|b_1|^2 - 1) + \mu(|x|^2 - r^2) + 2\langle \Lambda, x' - b_1 \rangle$$

to obtain the differential equations which govern the extremals:

$$\mu x - \Lambda' = 0, \tag{10}$$

$$\lambda b_1 - b_1'' = \Lambda. \tag{11}$$

Combining these equations yields

$$\lambda' b_1 + \lambda b_1' - b_1''' = \mu x. \tag{12}$$

The derivatives of b_1 expressed in the Darboux basis are given by

$$b_1' = \kappa_g b_2 - \frac{1}{r} b_3, \tag{13}$$

$$b_1'' = \kappa_g' b_2 - \left(\kappa_g^2 + \frac{1}{r^2}\right) b_1, \tag{14}$$

$$b_1''' = (-3\kappa_g \kappa_g') b_1 + \left(\kappa_g'' - \kappa_g^3 - \frac{1}{r^2}\kappa_g\right) b_2 + \frac{1}{r}\left(\kappa_g^2 + \frac{1}{r^2}\right) b_3. \tag{15}$$

Substituting these derivatives and $x = rb_3$ into (12) and rearranging gives

$$(\lambda' + 3\kappa_g\kappa_g')b_1 + \left(\lambda\kappa_g - \kappa_g'' + \kappa_g^3 + \frac{1}{r^2}\kappa_g\right)b_2 - \left(\frac{\lambda}{r} + \mu r + \frac{1}{r}\left(\kappa_g^2 + \frac{1}{r^2}\right)\right)b_3 = 0.$$

Finally, the linear independence of the vectors b_1, b_2 and b_3 implies that

$$\lambda = -\tfrac{3}{2}\kappa_g^2 + C \tag{16}$$

and

$$\kappa_g'' + \tfrac{1}{2}\kappa_g^3 - \left(C + \frac{1}{r^2}\right)\kappa_g = 0. \tag{17}$$

In order to determine the constant C in terms of the tension parameter σ, we consider the boundary condition

$$F(l) - \frac{\partial F}{\partial x'}(l)x'(l) - \frac{\partial F}{\partial b_1'}(l)b_1'(l) = 0$$

for the extremal x. This condition is implied by the fact that the total length l of the curve is variable in the variation (see, for example, [1]). Thus,

$$-\kappa_g^2(l) - \frac{1}{r^2} + \delta - 2\langle\Lambda(l), x'(l)\rangle = 0. \tag{18}$$

Substituting Λ according to (11) into the scalar product $\langle\Lambda, x'\rangle$ yields

$$\begin{aligned}\langle\Lambda(l), x'(l)\rangle &= \langle\lambda b_1(l), b_1(l)\rangle - \langle b_1''(l), b_1(l)\rangle \\ &= \lambda + (\kappa_g(l))^2 + \frac{1}{r^2} \\ &= -\tfrac{1}{2}(\kappa_g(l))^2 + \frac{1}{r^2} + C.\end{aligned}$$

Substituting this expression for the scalar product into (18), we obtain

$$C + \frac{1}{r^2} = \frac{1}{2}\left(\delta - \frac{1}{r^2}\right). \tag{19}$$

These results are summarized in the following theorem.

THEOREM 1

An elastic curve x under tension σ on the sphere of radius r satisfies the differential equations

$$\begin{pmatrix} x_1' \\ x_2' \\ x_3' \end{pmatrix} = \begin{pmatrix} 0 & 1/r & 0 \\ -1/r & 0 & \kappa_g \\ 0 & -\kappa_g & 0 \end{pmatrix} \begin{pmatrix} x_1 \\ x_2 \\ x_3 \end{pmatrix}, \tag{20}$$

where $x_1 = x$, $x_2 = rx'$, $x_3 = x \times x'$ and where the geodesic curvature κ_g of x is a solution of

$$\kappa_g'' + \tfrac{1}{2}\kappa_g^3 + \left(\frac{1}{r^2} - \frac{\sigma}{2}\right)\kappa_g = 0. \tag{21}$$

The curvature of a spherical elastic curve can be obtained from (7) and the fact that the normal curvature of spherical curves is constant. The squared torsion of a spherical elastica can be expressed as a rational function of its curvature.

THEOREM 2

The curvature κ and the torsion τ of a spherical elastic curve obey the relation:

$$r^2\tau^2\kappa^2 = -\tfrac{1}{4}\kappa^4 - \frac{1}{2}\left(\frac{1}{r^2} - \sigma\right)\kappa^2 + \frac{1}{r^2}\left(\frac{3}{4} - \frac{\sigma}{2}\right) + C_1.$$

Proof

For the invariants κ and τ of an arc length parametrized curve x in $\mathbb{R}^3$, the relation

$$\tau\kappa^2 = [b_1, b_1', b_1''] \tag{22}$$

holds, where [a, b, c] denotes the determinant of three vectors in $\mathbb{R}^3$.

For a spherical curve, b_1' and b_1'' can be expressed in the Darboux basis as follows:

$$b_1' = \kappa_g b_2 - \frac{1}{r} b_3,$$

$$b_1'' = -\left(\frac{1}{r^2} + \kappa_g^2\right) b_1 + \kappa_g' b_2.$$

Substituting the derivatives into (22) and squaring yields

$$\tau^2\kappa^4 = \frac{1}{r^2}(\kappa_g')^2.$$

Since the differential equation (21) can be integrated to

$$(\kappa_g')^2 = C_1 - \tfrac{1}{4}\kappa_g^4 - \left(\frac{1}{r^2} - \frac{\sigma}{2}\right)\kappa_g^2,$$

one obtains the claimed equation using (7). □

4. Tracking elastic curves on the sphere

The problem we consider here is that of numerically integrating equations (20) and (21) in theorem 1. One can of course simply integrate the equations using a standard numerical package, such as an IMSL Runge–Kutta routine. However, the system of equations possesses a very special structure. As pointed out in [3], equation (21) may be integrated directly in terms of Jacobi's elliptic functions. We give more details of this process in the next section, where we classify the various extremals. As for equation (20), we note that the components of the state vector $[x_1^T, x_2^T, x_3^T]^T$ satisfy algebraic constraints consistent with the fact that the matrix $[x_1, x_2, x_3]$ is simply a multiple of r, of a rotation matrix. When a standard integration package is applied to the set of differential equations (20) and (21), these constraints are not preserved exactly, and in particular the norm of the vector x_1 will not remain at the constant value r. This is a particularly important fact when we wish to integrate the equations over a large number of time steps and visualize the resulting curves.

We have therefore made use of a new class of integration algorithms, developed by Crouch and Grossman [9], and Crouch et al. [8], which do indeed preserve such structures. The algorithms are therefore called geometrically exact [7]. We briefly indicate the important aspects of these geometrically stable algorithms which pertain to equations (20) and (21). Suppose that we wish to numerically integrate an ordinary differential equation on $\mathbb{R}^n$ given by the equations

$$\dot{x}(t) = F(t, x(t)), \quad x \in \mathbb{R}^n, \; x(0) = x_0, \tag{23}$$

where

$$F(t, x) = \sum_{j=1}^{N} a^j(t, x) A_j(x), \tag{24}$$

$n \geq N$, A_j are vector fields on $\mathbb{R}^n$ and a^j are functions on $\mathbb{R} \times \mathbb{R}^n$. Suppose that in addition we are given a set of functions on $\mathbb{R}^n$ whose numerical values are constant along solutions of the equation (23) and that the level sets of these functions are manifolds. Denote the level set through x_0 by M. It is convenient to assume the slightly stronger assumption that the vector fields A_j are everywhere tangent to M. We also assume that there is an oracle that can integrate any vector field of the following form, to any desired accuracy:

$$Z(x) = \sum_{j=1}^{N} \alpha^j A_j(x). \tag{25}$$

Here, α^j are real numbers. We define vector fields F^p by setting:

$$F^p(x) = \sum_{j=1}^{N} a^j(p) A_j(x)$$

and note that F^p is simply the vector field F with coefficients "frozen" at the point p. If we denote the flow of any vector field Z by $(t, x) \to \theta_Z(t, x)$, $\mathbb{R} \times \mathbb{R}^n \to \mathbb{R}^n$, then since the vector fields A_j are everywhere tangent to M, it follows that $x \in M$ implies that $\theta_{F^p}(t, x) \in M$ for all p and for all t for which the flow is defined.

We now introduce the (explicit) geometrically exact Runge–Kutta algorithms as described in [9]. Let $x_k = x(t_k)$ be a point of the integral curve x of (23). Then, define vector fields on $\mathbb{R}^n$ by freezing coefficients of F at various points as follows:

$$F_1(x) = \sum_{j=1}^{N} a^j(t_k, x_k) A_j(x),$$

$$F_2(x) = \sum_{j=1}^{N} a^j(t_k + hc_{21}, \theta_{F_1}(hc_{21}, x_k)) A_j(x),$$

$$F_3(x) = \sum_{j=1}^{N} a^j(t_k + h(c_{31} + c_{32}), \theta_{F_2}(hc_{32}, \theta_{F_1}(hc_{31}, p))) A_j(x),$$

etc. Second, we define the numerical integration algorithm via an update rule:

$$x_{k+1} = \theta_{F_r}(hc_r, \theta_{F_{r-1}}(hc_{r-1}, \ldots, \theta_{F_1}(hc_1, x_k))), \tag{26}$$

where h is the "step length" and c_i and c_{ij} are constants to be determined. These constants are determined from the "consistency equations", obtained by making the Taylor expansions in h, about $h = 0$, of both sides of (26), using on the left-hand side the expression $x_{k+1} = \theta_F(h, x_k)$. If the coefficients of h^i agree up to $i = q$, then q is said to be *order* of the resulting algorithm. Note that in general we have $r \geq q$, while for classical Runge–Kutta schemes we can always take $r = q$. Note also that the update rule defined by equation (26) has the property that if x_k lies in M, then so does x_{k+1} since each flow is defined by a vector field F with frozen coefficients. In the special case where $n = N$, $M = \mathbb{R}^n$ and $A_i = e_i$ is the standard ith basis vector in $\mathbb{R}^n$, the algorithm reduces to the form of a classical explicit Runge–Kutta algorithm.

In the paper [9], the consistency equations are derived for the geometrically exact Runge–Kutta algorithms via a careful geometric analysis of equations (26). The results show that a geometrically exact third-order explicit Runge–Kutta algorithm can be obtained for $r = 3$ and is determined by five independent consistency equations,

in the six constants defining the algorithm. The equations have multiple solutions, all of which are solutions to the equations which determine the classical explicit Runge–Kutta algorithms. Thus, all solutions define classical algorithms, but the solutions are not ones traditionally found in the literature. We have used the following solution of all five equations:

$$c_1 = 1, \quad c_2 = -2/3, \quad c_3 = 2/3,$$
$$c_{21} = -1/24, \quad c_{31} = 161/24, \quad c_{32} = -6.$$

In the special case of the set of equations (20) and (21) defining the elastica on a sphere, we use a hybrid algorithm in which equations (20) are integrated, using the third-order geometrically exact Runge–Kutta algorithm described above, by freezing the coefficients κ_g. These coefficients are then updated by integrating equation (21) using elliptic functions.

In equation (20), M is the three-dimensional submanifold of $\mathbb{R}^9$ determined by the equations

$$\langle x_1, x_1 \rangle = r^2, \quad \langle x_1, x_2 \rangle = 0, \quad \langle x_1, x_3 \rangle = 0,$$
$$\langle x_2, x_2 \rangle = 1, \quad \langle x_2, x_3 \rangle = 0, \quad \langle x_3, x_3 \rangle = 1.$$

The solutions of (20) for any initial condition $x(0) = x_0 \in M$ lie completely in M. This follows from the fact that the functions

$$f_1 = \langle x_1, x_1 \rangle, \quad f_2 = \langle x_1, x_2 \rangle, \quad f_3 = \langle x_1, x_3 \rangle,$$
$$f_4 = \langle x_2, x_2 \rangle, \quad f_5 = \langle x_2, x_2 \rangle, \quad f_6 = \langle x_3, x_3 \rangle$$

satisfy the system of differential equations

$$f_1' = 2f_2,$$
$$f_2' = f_4 + \kappa_g f_3 - (1/r^2) f_1,$$
$$f_3' = f_5 - \kappa_g f_2,$$
$$f_4' = 2\kappa_g f_5 - (2/r^2) f_2,$$
$$f_5' = \kappa_g f_6 - (1/r^2) f_3 - \kappa_g f_4,$$
$$f_6' = -2\kappa_g f_5,$$

which has the unique solution

$$f_1 = r^2, \quad f_2 = 0, \quad f_3 = 0, \quad f_4 = 1, \quad f_5 = 0, \quad f_6 = 1.$$

Since this argument does not specify the function κ_g, it follows that the flows of the vector fields $F_1 - F_3$ with frozen coefficients are mappings into M as needed in formula (26).

Furthermore, the vector fields A_j in equation (20) are linear, so that F is given by an expression of the form

$$F(x) = \sum_{j=1}^{N} b^j(t, x) B_j x, \tag{27}$$

where B_j are matrices and b^j are functions. Freezing the functions b^j to values β^j yields a system of linear differential equations with constant coefficients:

$$\dot{x} = \left(\sum_{j=1}^{N} \beta^j B_j \right) x. \tag{28}$$

Thus, the flow θ_{F_i} of the vector field F_i $(i = 1, 2, 3)$ is given by

$$\theta_{F_i}(t, q) = \exp(tC_i)q$$

and (26) takes the special form

$$x_{k+1} = \exp(c_3 h C_3) \cdot \exp(c_2 h C_2) \cdot \exp(c_1 h C_1) \cdot x_k.$$

Since $b^1 = 1/r$ is constant and $b^2 = \kappa_g$ depends only on t, the matrices C_i are given by

$$C_1 = C(t_k), \quad C_2 = C(t_k + hc_{21}), \quad C_3 = C(t_k + h(c_{31} + c_{32})),$$

where $C(t) := \sum_{j=1}^{2} b^j(t) B_j$. C can be considered as a 3×3 skew symmetric matrix with matrix components that are themselves 3×3 matrices. Therefore, the standard formula for the exponential of a 3×3 skew symmetric matrix can be used to compute the flow of each vector field:

$$\exp(t\phi S(c)) = I + \sin(t\phi) S(c) + (1 - \cos(t\phi)) S(c)^2,$$

where $S(c)$ is the skew symmetric matrix satisfying $S(a)b = b \times a$, and $|c| = 1$.

Regarding the performance of the geometrically stable integration method, it is clear that the method is computationally more expensive than a classical algorithm with the same number of stages and step length. The exact cost of the new integration scheme can be found in [7]. However, if we compare the performance of the geometrically stable method with the classical fourth-order Runge–Kutta algorithm on the problem of spherical elastica, it turns out that a slightly increased step length for the new method suffices to outperform the classical integration method. Using MATLAB implementations of both algorithms, we found that one can statistically achieve the same performance by using an increased step length of $h \approx 1.3038 h_{RK}$

for the new method. Taking into account that the proposed algorithm not only delivers points that lie exactly on the sphere but that are also approximately equally spaced along the tracked curve, the geometrically stable method seems to be a good choice for the integration of spherical elastica.

A performance comparison of the new integration scheme with a more sophisticated classical method, the IMSL Runge–Kutta implementation, can be found in [8].

5. Classification of spherical elastica

Acting on the suggestion of Bernoulli, Euler derived differential equations for plane elastica and classified the fundamental forms of these curves (see [10, 14]). A curvature analysis of the various fundamental cases has been given in [4].

In this section, we classify the forms of spherical elastica based on the differential equation (21) for the geodesic curvature. This equation is of the same form as the equation for the curvature of plane elastica and can be solved in terms of Jacobi's elliptic functions in the form

$$\kappa_g(s) = \kappa_m \mathrm{dn}(\kappa_m(s - s_m)/2 \,|\, l^2),$$

where the positive parameter l^2 of the elliptic function is given by

$$l^2 = \frac{2(\kappa_m^2 + 2/r^2 - \sigma)}{\kappa_m^2} \tag{29}$$

(see [4]). The parameter κ_m represents the amplitude of the periodic curvature function and s_m denotes the value at which $\kappa(s_m) = \kappa_m$.

To obtain a representation of the curvature in terms of Jacobi's functions with parameter l^2 smaller than 1, ones uses the formula

$$\kappa_g(s) = \kappa_m \mathrm{cn}\left(\sqrt{(\kappa_m^2 + 2/r^2 - \sigma/2}(s - s_m) \,\middle|\, \frac{1}{l^2}\right), \tag{30}$$

if $\sigma < 0.5\kappa_m^2 + 2/r^2$. Since the function cn has zeros while dn is positive, the above case distinction reflects the main division of elastic curves into those where the geodesic curvature changes sign and the other with constant sign of their geodesic curvature.

The change of the forms of spherical elastica while κ_m is fixed and σ increases is shown by figures 1–8. The maximum value of the tension parameter σ for a real elastic curve on a sphere is, according to (29), $\sigma = \kappa_m^2 + 2/r^2$. This choice of σ corresponds to the dashed circle that is shown in all figures for the purpose of orientation. The second curve in figure 1 has a negative tension parameter of high absolute value ($\sigma = -10000$). In comparison to figure 2, where $\sigma = -30$, we observe

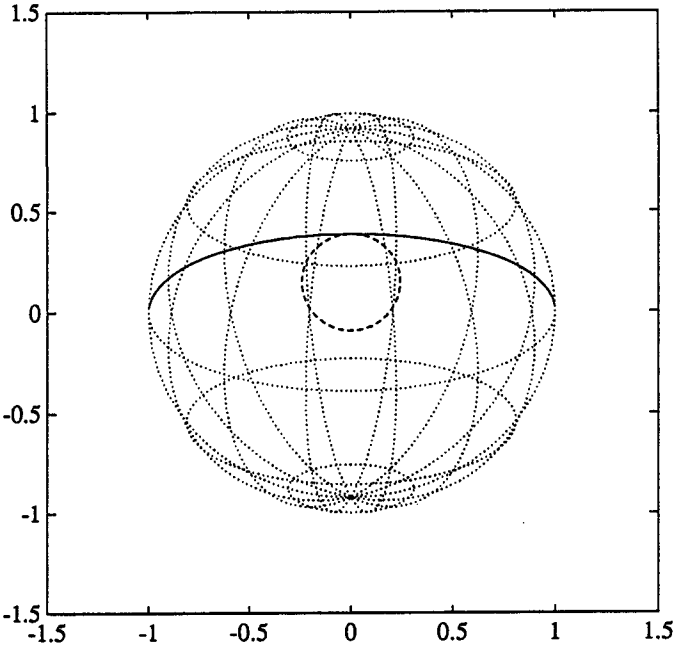

Figure 1. $\kappa_m = 4$, $\sigma = -10000$.

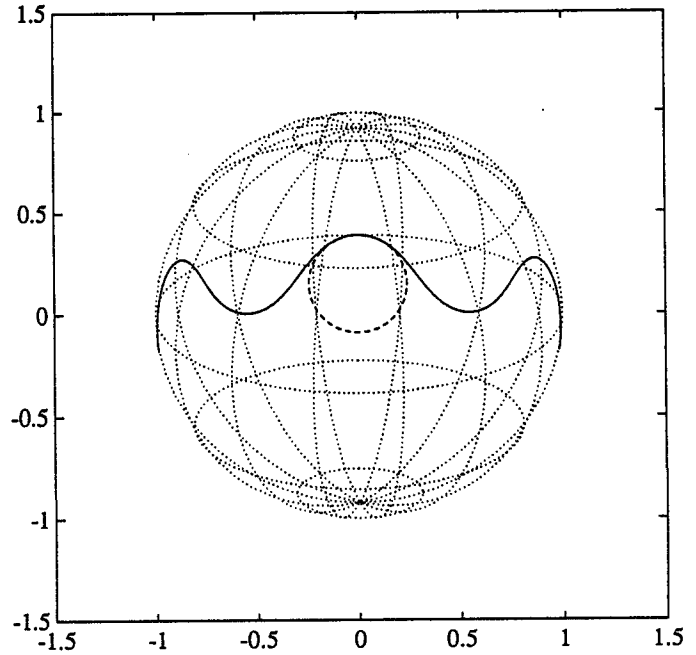

Figure 2. $\kappa_m = 4$, $\sigma = -30$.

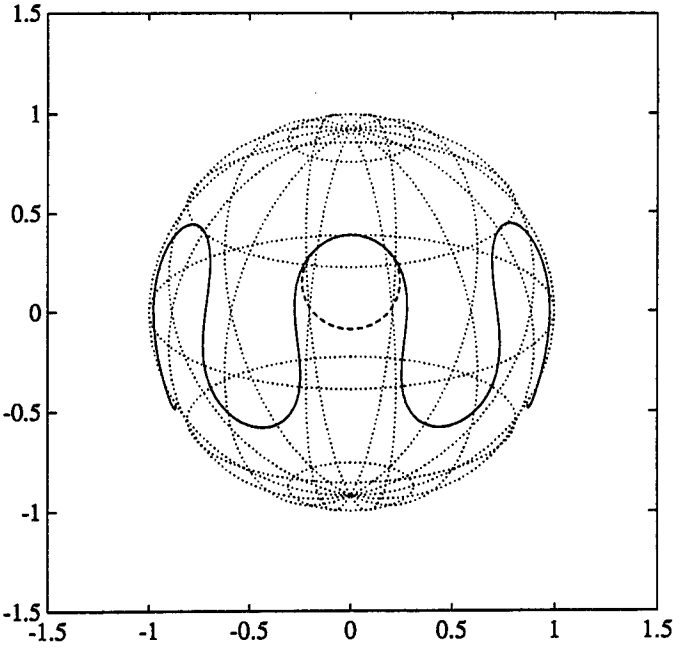

Figure 3. $\kappa_m = 4$, $\sigma = 2$.

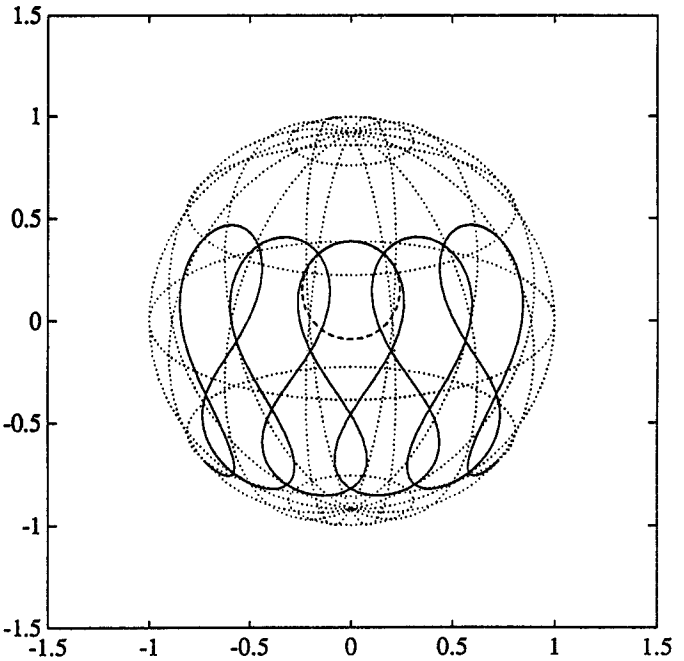

Figure 4. $\kappa_m = 4$, $\sigma = 6.8$.

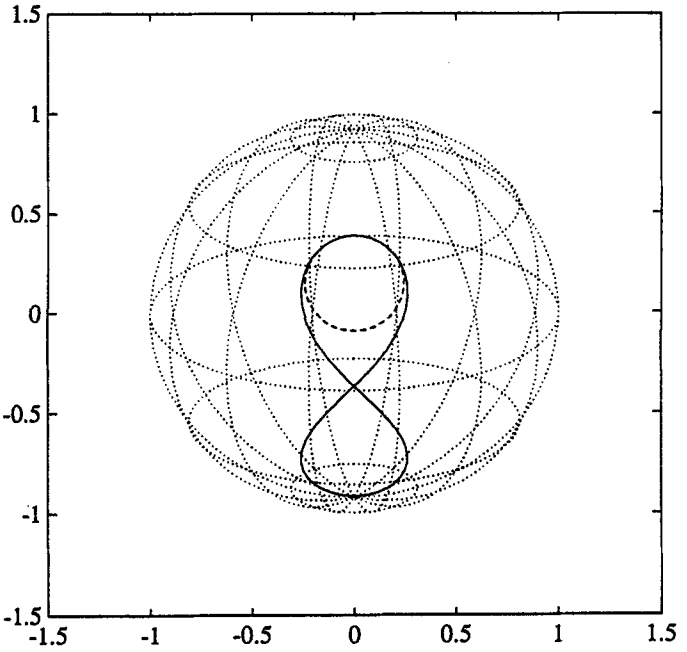

Figure 5. $\kappa_m = 4$, $\sigma = 7.8489$.

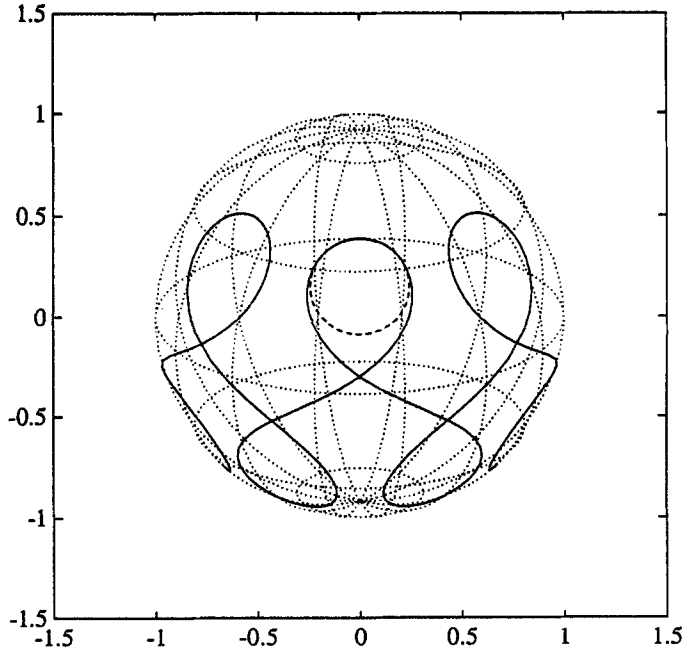

Figure 6. $\kappa_m = 4$, $\sigma = 9.04$.

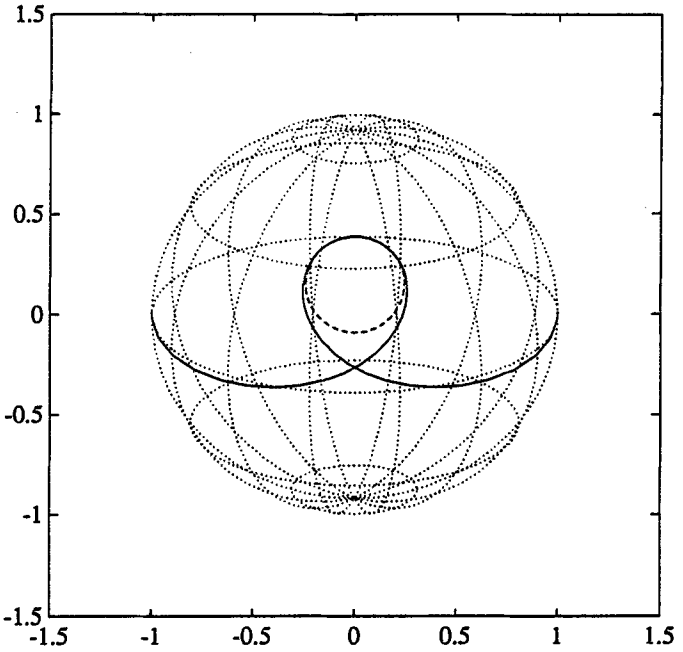

Figure 7. $\kappa_m = 4$, $\sigma = 10$.

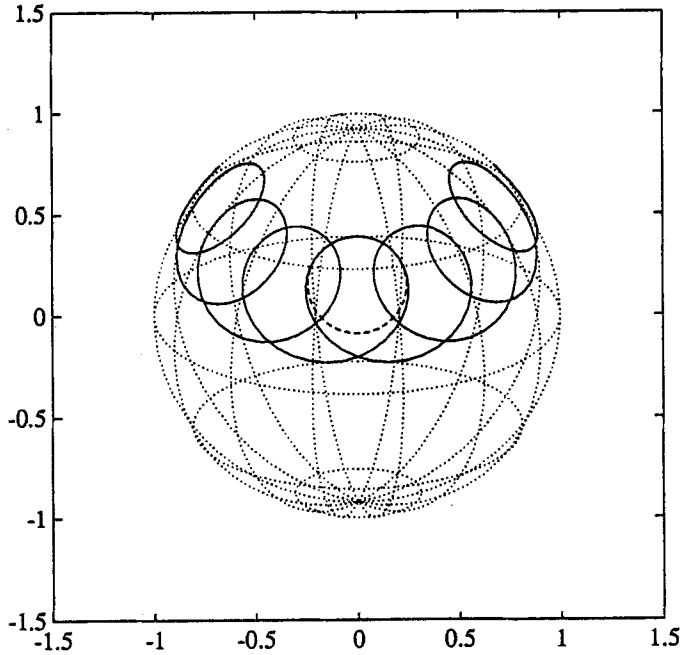

Figure 8. $\kappa_m = 4$, $\sigma = 11.92$.

that decreasing the tension parameter has the effect of lowering the amplitude of the curves as it is known from the Euclidean case (see [4]). The oscillation of the curve in figure 1 is of too low amplitude to be visually observed and the curve can not be distinguished from the geodesic determined by the initial condition. (Note that the geodesic curvature (30) is far from becoming flat for $\sigma \to -\infty$, but in fact approaches a cos function that oscillates with a period that decreases with σ.)

A curve with a positive tension parameter is shown in fig. 3, where $\sigma = 2/r^2 = 2$. The displayed curve is a special case because the parameter $1/l^2 = 1/2$. Here, the geodesic curvature is given by the lemniscate function

$$\kappa_g(s) = \kappa_m \text{coslemn}(\kappa_m(s - s_m)/2).$$

In figures 4 and 5, it is illustrated that with increasing positive σ the bays of the curves start to overlap until a figure-8 configuration is reached where all double points of the curve coincide. This happens for a parameter $\sigma \approx 7.849$.

While σ increases further, the curve proceeds through the figure-8 shape, forming a series of loops with alternating sign of geodesic curvature (see figure 6). These loops recede from each other until, in the limiting case when $\sigma = 2/r^2 + 0.5\kappa_m^2$, the curve forms a single loop (see figure 7). Here, the geodesic curvature is given by

$$\kappa_g(s) = \kappa_m \text{sech}(\kappa_m(s - s_m)/2).$$

Figure 8 shows that the single loop transforms into a series of loops with the same sign of geodesic curvature. With increasing σ, the loops come closer together and finally collapse into a circle when $\sigma = 2/r^2 + \kappa_m^2$.

References

[1] O. Bolza, *Vorlesungen über Variationsrechnung* (Koehler und Amelang, Leipzig, 1949).

[2] A.M. Bruckstein and A.N. Netravali, On minimal energy trajectories, Comp. Vision, Graphics, and Image Proc. 49(1990)283–296.

[3] G. Brunnett, Properties of minimal energy splines, in: *Curve and Surface Design*, ed. H. Hagen (SIAM, 1992) pp. 3–22.

[4] G. Brunnett, A new characterization of plane elastica, in: *Mathematical Methods in Computer Aided Design II*, ed. T. Lyche and L. Schumaker (Academic Press, 1992) pp. 43–56.

[5] G. Brunnet and J. Kiefer, Interpolation with minimal energy splines, to be published in CAD.

[6] M.P. do Carmo, *Differential Geometry of Curves and Surfaces* (Prentice–Hall, 1976).

[7] P.E. Crouch, R. Grossman and Y. Yan, A third order Runge–Kutta algorithm on a manifold, submitted to BIT (1992).

[8] P.E. Crouch, Y. Yan and R. Grossman, On the numerical integration of the synamic attitude equations, *Proc. IEEE CDC Conf.*, Tucson, AZ (1992), to appear.

[9] P.E. Crouch and R. Grossman, Numerical integration of ordinary differential equations on manifolds, J. Nonlin. Sci. (1991), to appear.

[10] L. Euler, *Additamentum De Curvis Elasticis*, Methodus Inveniendi Lineas Curvas Maximi Minimive Proprietate Gaudentes, Ser. 1, Vol. 24, Lausanne (1744).

]11] J. Hoschek and G. Seemann, Spherical splines, Math. Mod. Numer. Anal. 26(1992)1–22.
[12] J. Jackson and P.E. Crouch, Dynamic interpolation and application to flight control, J. Guidance, Control and Dynamics 14(1991)814–822.
[13] E. Jou and W. Han, Minimal energy splines with various end constraints, in: *Curve and Surface Design*, ed. H. Hagen (SIAM, 1992) pp. 23–30.
[14] A.E.H. Love, *A Treatise on the Mathematical Theory of Elasticity*, 4th ed. (Cambridge University Press, 1927).
[15] H. Moreton and C. Sequin, Surface design with minimum energy networks, ACM Comp. Graphics, *Proc. SIGGRAPH* (1991).
[16] G. Nielson, Bernstein/Bézier curves and splines on spheres based upon a spherical de Casteljau algorithm, Technical Report TR-88-028, Arizona State University (1988).
[17] L. Noakes, G. Heinzinger and B. Paden, Cubic splines on curved spaces, IMA J. Math. Control Inf. 6(1989)465–473.
[18] K. Shoemaker, Animating rotation with quaternion curves, ACM Comp. Graphics 10, *Proc. SIGGRAPH'85* (1985) pp. 245–254.
[19] K. Strubecker, *Differentialgeometrie I–III*, Sammlung Göschen (de Gruyter, Berlin, 1969).